

Very high-precision absolute surface metrology gauges for building and qualifying SIM testbed interferometer compound optics

Yekta Gürsel

Jet Propulsion Laboratory, California Institute of Technology, Pasadena, California, U.S.A.

ABSTRACT

The Stellar Interferometry Mission (SIM), and particularly one of its testbeds [the Micro-Arc-Second Metrology Testbed (MAMTB)] require compound optical pieces the construction and qualification of which, in turn, require very high-precision absolute surface metrology gauges.

There are many designs examined in the literature for absolute surface metrology gauges. Some of these use a standard surface gauge and perform repeated measurements in various piece orientations to measure and calibrate several optical pieces simultaneously. As the pieces get flatter and flatter, these suffer from more and more of accumulating subtraction errors. These can not measure pieces that has a retro-reflector mounted on them in absolute terms.

There is another class of surface metrology gauges that avoid most of these problems. These gauges use a 3-fiber, laser-light and white-light, fiber-tip interferometer to calibrate a flat absolutely without subtraction and use this flat in a split-beam single-fiber, fiber interferometer to measure and calibrate compound optical pieces, like flat mirrors with retro-reflectors embedded in them.

We have been building a system as described above. Our 3-fiber interferometer is in alignment and displaying the first fringes and delivering phase-maps. The split-beam, single-fiber interferometer is under construction. Both interferometers are designed to operate in vacuum, mounted on one top of another in a mezzanine-type arrangement in our 4 ft. vacuum chamber. In addition, a smaller white light interferometer has been built to manufacture some of the compound optics while the main gauges are being developed. One previously glued siderostat with a corner cube has been measured and two new siderostats with corner cubes have been assembled and measured using this interferometer.

In this paper, the details of the design, construction and performance of these triplet of interferometers are presented.

Keywords: Spaceborne interferometry, absolute surface gauges, siderostat, retro-reflector

1. INTRODUCTION

The Space Interferometry Mission (SIM) spacecraft designs consists of three high resolution stellar interferometers with variable-length base-lines for micro-arc-second accuracy astrometric measurements. These stellar interferometers require picometer accuracy one dimensional metrology gauges, very high accuracy surface metrology gauges and 3-dimensional metrology gauges to measure the required distances or to calibrate the fiducials that define the end points of the interferometric paths. The absolute metrology gauges required by these interferometers can be considerably less accurate due to the careful design of the astrometric interferometers and the fiducials on the spacecraft.

Each stellar interferometer on the SIM spacecraft has at least two siderostats that track the observed star. The siderostats are the first point of contact for the starlight before it enters the instrument. One part of

Further author information:

E-mail: Yekta.Gursel@jpl.nasa.gov, Telephone: 1 818 354 3645, Address: Mail Stop 306-388, Jet Propulsion Laboratory, 4800 Oak Grove Dr., Pasadena, CA, 91109, U.S.A.

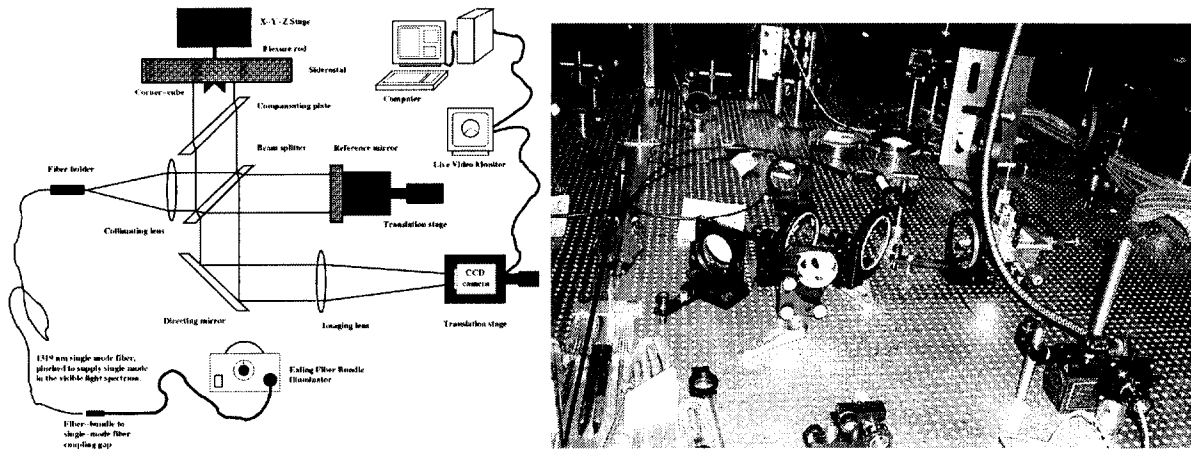


Figure 1. The diagram and the picture of the white-light assembly interferometer.

this starlight coming from one of the siderostats is combined with another part of it coming from the other siderostat, and resulting interferometric white light fringe is tracked to determine the angle of the star.

In order to form the fringe, the phases of the light reflected by the siderostats have to be unaltered until the light is recombined. Since there are many optical elements in the starlight path and the relatively-flexible spacecraft expands and shrinks as time passes, the optical path-lengths from the beam combiner to the individual siderostats have to be known, in order to compensate for these changes.

An internal metrology system tracks the optical pathlengths from the beam combiner to the siderostats. The siderostats do not face the metrology beam directly; They are angled to bring the light from the observed star in. There has to be a fiducial element on the siderostat that reflects the metrology light back into the metrology system independent of the angle of the siderostat while accurately locating the reflective surface of the siderostat on which the incident starlight falls.

The fiducial element is usually a hollow, corner-cube retro-reflector, the optical corner of which is to coincide with the reflective surface of the siderostat. It is very difficult to manufacture an optical piece like this to sub-nanometer accuracy. They are usually made to micron-accuracy, that is to say, the estimated separation between the actual optical corner of the retro-reflector and the siderostat-surface is about a micrometer. SIM⁴ requires that this distance to be known to at least to 1 nm.

In what follows, a triple-gauge system that is used to manufacture such optical pieces, and subsequently to measure them to sub-nanometer accuracy is described. The first interferometer in the system is the assembly white-light interferometer. The next one is the reference flat absolute calibrator, known as the 3-fiber gauge. The final step in the process is performed in the split-fiber beam, single fiber interferometer which uses the calibrates reference flat to measure the corner-cube-siderostat assembly.

2. THE WHITE-LIGHT ASSEMBLY INTERFEROMETER

The white-light assembly interferometer is a Michelson type interferometer with many improvements to make corner-cube to siderostat attaching operation as easy and accurate as possible.

Fig. 1 shows a diagram and a picture of the white-light assembly interferometer. The light source is an Ealing fiber-bundle illuminator that supplies cool (infrared filtered) white-light from a standard 150 W slide-projector lamp. The output of the bundle is simply brought close to the input of the 1319 nm, 9 μm core diameter, single-mode fiber which is aligned to accept most of the light. A small section of the single-mode fiber is wound into a tight, single-turn loop and pinched to make the fiber single mode in the visible spectrum. The output of the fiber is collimated and goes into the Michelson interferometer with a compensating plate. The reference

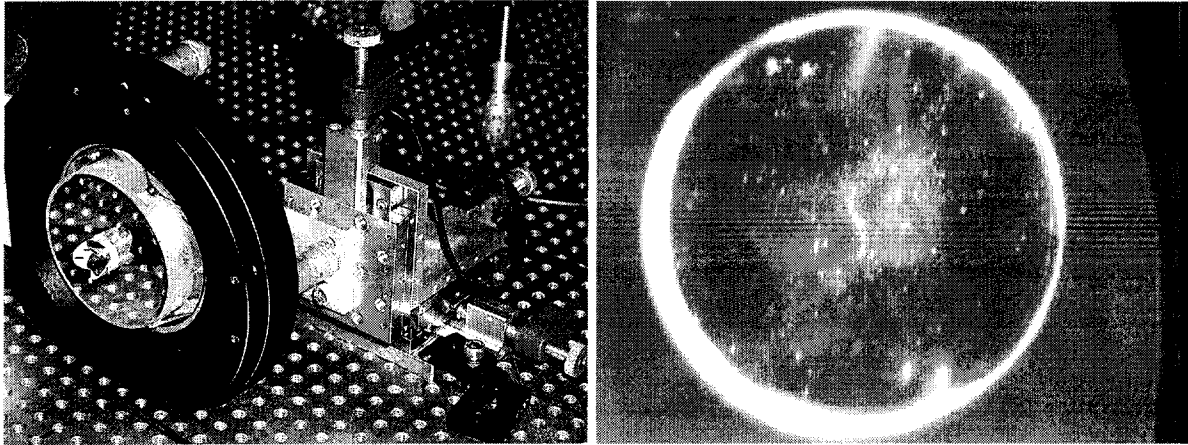


Figure 2. Left: The siderostat and the hollow, corner-cube retro-reflector. Right: The part of the siderostat and the retro-reflector as seen by the interferometer CCD camera.

mirror is in one of the arms of the interferometer while the siderostat and the corner cube at its center sits in the other arm. A digital micrometer on the reference-mirror translation stage is used only for calibration.

Fig. 2 shows a close-up picture of the siderostat with the corner cube. The siderostat is mounted into a standard 4" Newport mirror mount by an adapter that holds the siderostat through flexures.³ The cylindrical corner cube slides into a hole at the center of the siderostat and a specially designed flexure rod³ connects the corner-cube retro-reflector to an X-Y-Z stage equipped with pico-motors behind the mirror mount.

The output of the interferometer is directed by a mirror to an imaging lens which images the siderostat-corner-cube assembly on to a monochrome CCD camera which is chosen for its low-light sensitivity. The output of the camera goes to a old Intel Pentium PC with a PCI bus compatible, Conexant Bt-848 chip based, 8-bit frame grabber. LINUX operating system with the readily available device drivers (bttv) complete the data system. The data is analyzed on the same PC in real-time by algorithms and software developed by the author.

Fig. 2 also shows the part of the siderostat and the corner-cube retro-reflector at the center as seen by the interferometer camera. In this white-light picture, the joining lines of the retro-reflector, the dust particles on the retro-reflector faces left by the packaging of the retro-reflector, the glue smudge at the center due to a manufacturing defect as well as the horizontal white-light fringes near final alignment are clearly visible.

2.1. The optimization of alignment

To align the white-light assembly interferometer from scratch, a diode laser is used. The fiber input to the interferometer is essential for changing the light source without losing interferometer alignment. The diode laser is coupled into the fiber by simply pointing it into the fiber tip. The intense, more coherent light from the laser diode makes finding of the first fringes very easy.

Note that the retro-reflector sends the interferometer beam right back on itself automatically independent of the direction of the beam, while the siderostat has to be perpendicular to the interferometer beam to accomplish the same. This presents a problem with the alignment of the whole system all together. The problem is easily solved by first aligning the interferometer using only the siderostat part.

To match the fringes seen in the retro-reflector and the siderostat, the reference-mirror tip and tilt directions are used to move the fringes seen in the retro-reflector next, and then the siderostat tip and tilt directions are moved to align the siderostat and the retro-reflector fringes together.

The laser diode is then swept in frequency while moving the reference-mirror translation stage to make the path-lengths of the arms nearly equal. The white-light fiber bundle is then brought back to the input to search

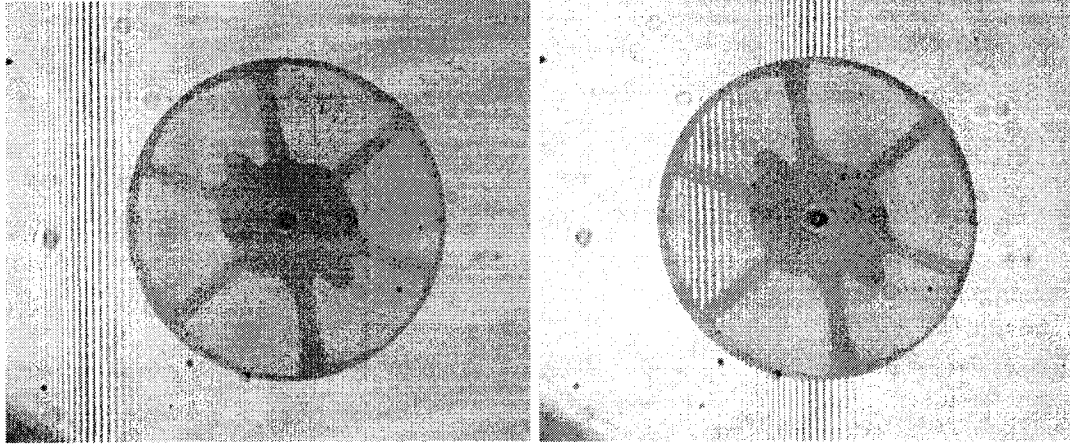


Figure 3. Left: White light fringe cluster on the siderostat. Right: The fringe cluster breaks over the retro-reflector; siderostat is not co-planar with the retro-reflector.

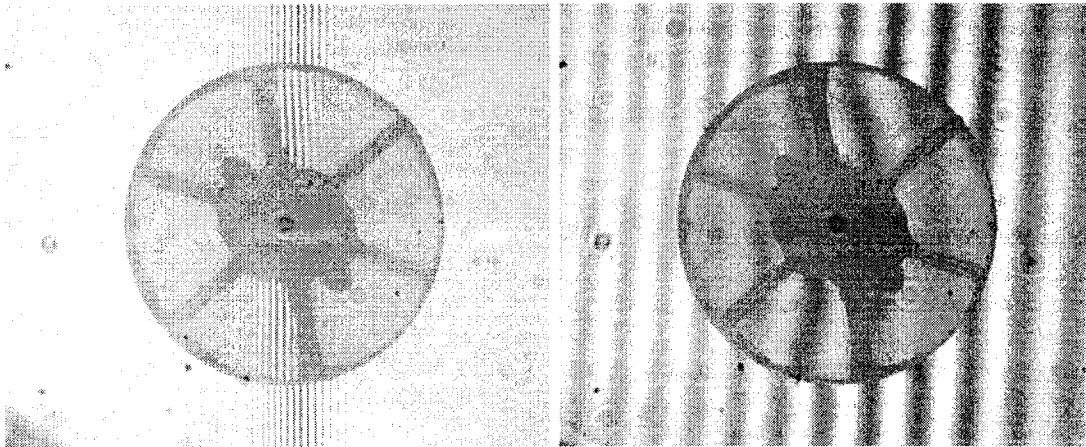


Figure 4. Left: Coarse alignment state. The fringe cluster is continuous across the retro-reflector. Right: The reference mirror is tilted back revealing minor misalignment.

for the white-light fringes on the siderostat which are readily found by moving the translation stage of the reference mirror.

To align the optical corner of the corner-cube retro-reflector with the reflecting surface of the siderostat, first the X-Y stage is moved so that the retro-reflector slides easily without binding in its hole. Then, the z-stage is used to move the retro-reflector in the direction of the interferometer beam to find the white-light fringes seen in the retro-reflector.

For the best match between the optical corner of the retro-reflector and the reflective surface of the siderostat the central white light fringe has to pass through the center of the retro-reflector. This is the point where other schemes¹ that actually looked for the central dark fringe near “0-fringe” alignment had produced inferior alignment.

In the author’s scheme, the reference mirror is tilted slightly so that the white light fringes appear as a cluster on the siderostat first, as shown in Fig. 3. The reference-mirror translation stage is moved to bring these fringes

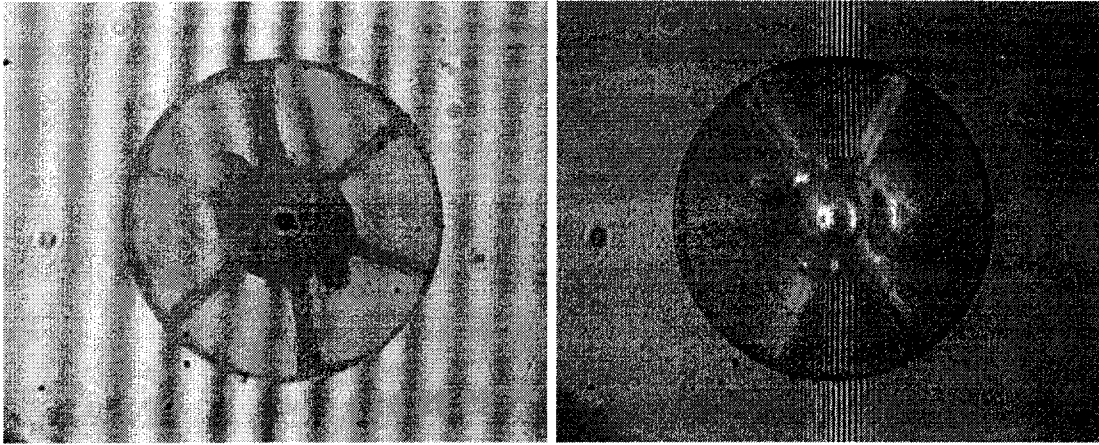


Figure 5. Left: Fine alignment state. The fringe cluster is continuous across the retro-reflector with enlarged spacing. Right: Aligned white-light fringes and the retro-reflector with a ball at the center.

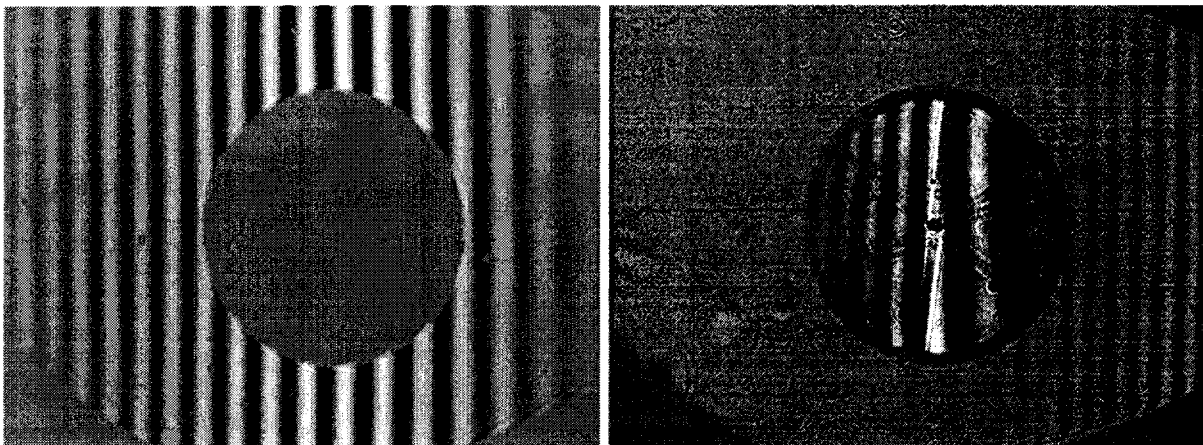


Figure 6. Left: White-light fringe cluster across the siderostat of an existing badly assembled siderostat-retro-reflector combination by another team in another interferometer. Right: White-light fringe cluster across the retro-reflector of the same badly assembled siderostat-retro-reflector combination.

over the retro-reflector. The siderostat and the optical corner of the retro-reflector is not co-planar initially. This causes the fringe band to break as shown also in Fig. 3. The Z-stage attached to the retro-reflector is moved to make the fringe band continuous as shown in Fig 4. The reference mirror is tilted back to reveal minor mis-alignments as shown in the same figure. Finally, Fig. 5 shows the final alignment state. The fringes through the retro-reflector are curved since it takes three reflections to go through it. This makes it about three times worse than the flatness of the siderostat if the retro-reflector faces are made with same flatness specifications. Note that this retro-reflector has a small ball glued at its center for other alignment purposes.

2.2. The monitoring of alignment

The first piece that was measured in the white-light assembly interferometer was a siderostat-retro-reflector combination which was glued by another team in another interferometer¹ over a year ago. The result was very surprising. The white light fringes did not even cross the retro-reflector when they were centered on the

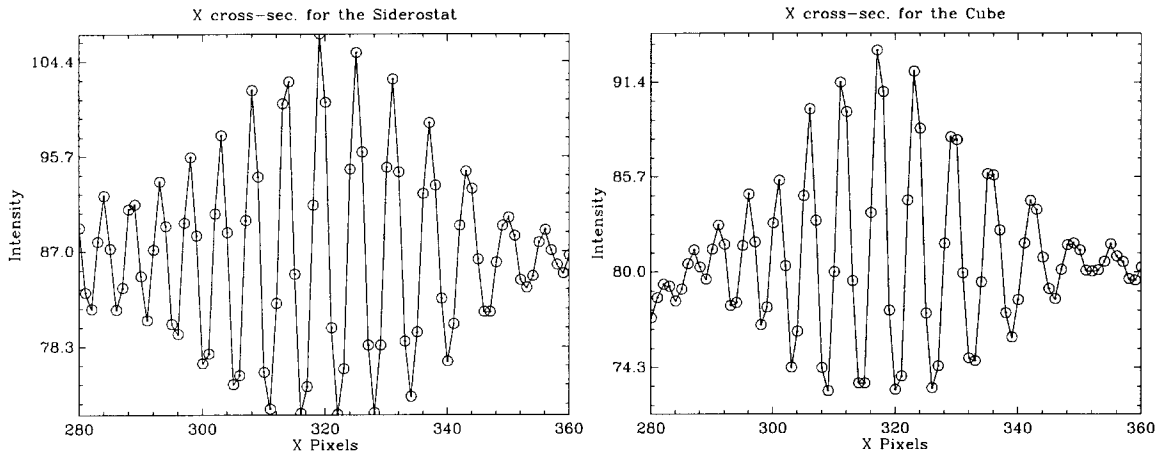


Figure 7. Left: Cross-section of the white light fringes across the siderostat. Right: Cross-section of the white light fringes across the retro-reflector.

siderostat. When there were fringes on the siderostat, the ones that were to be on the retro-reflector were not even on the same video screen. The fringe separation was measured carefully by the author using the digital micrometer on the translation stage of the reference mirror and was found to be offset by $6 \mu\text{m} \pm 0.5 \mu\text{m}$. The fringes corresponding to this siderostat-retro-reflector assembly are shown in Fig. 6.

Because of this, we have decided to use a very hard glue³ that is impossible to remove in the case of a mistake without damaging both optical pieces. This glue dries very slowly in about 24 hours. This necessitated semi-automated measurement and monitoring of the fringes. The author came up with a very fast fringe center algorithm that can locate the center of the fringe cluster down to better than 50 nm by looking at a cross-section of the white-light fringe cluster. When several locations across the cluster is monitored this way, the drifts of the order of 100 nm are easily seen and if necessary they are corrected. Usually a single cross-section across the siderostat and another one across the cube is sufficient as it is the longitudinal direction that drifts the most due to optical table expansion. The mirror mounts that control the tilts are much more stable and they do not drift significantly. More cross-sections can be computed if necessary for fully automated alignment.

Fig. 7 shows typical fringe cluster cross-sections in the white-light assembly interferometer with a monochrome CCD camera. The author's scheme of very fast fringe-cluster center location finding algorithm is based on amplitude modulated (AM) radio pulse envelope detection and timing. To find the center of the cluster, the fringe as shown is simply line-fitted to remove any trends, then it is full-wave rectified. The resulting waveform is optimally low-pass filtered with a sliding box-car filter to remove the "carrier" and the resulting "bell-shaped" envelope is fitted with an eighth order polynomial, and the maximum of the polynomial fit is located. This is the fringe center. This algorithm is very fast compared to the real-time video rate, allowing many cross-sections to be computed in real-time for automatic alignment.

Using the set-up and the algorithm described, we have assembled two siderostat-retro-reflector combinations. The computer has kept track of the alignment during the glue curing procedure, calculating fringe cluster centers and logging them. The fringe pictures are also saved at every half an hour to one hour intervals to make movies of the fringe movement for each assembly. The logged entries are transmitted via pager to the author at night providing coverage for 24 hours a day. The siderostat-surface to the optical corner of the retro-reflector distances have been found to be much less than 50 nm in both cases, meeting and exceeding all expectations.

3. THE 3-FIBER GAUGE

The next step in manufacturing and testing the SIM siderostat-retro-reflector assemblies is to absolutely measure flatness of non-curved optical pieces that are used to assemble high-precision retro-reflectors and to absolutely

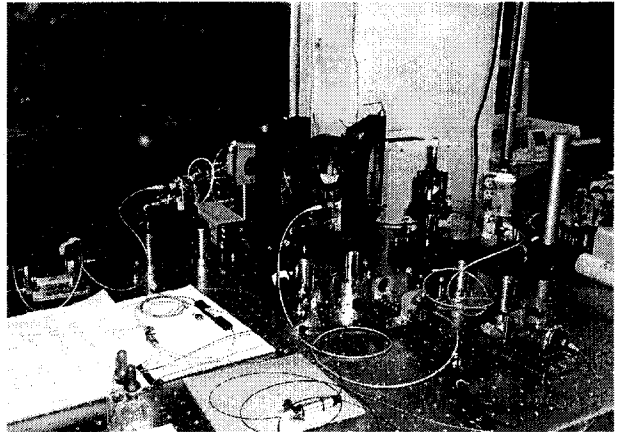
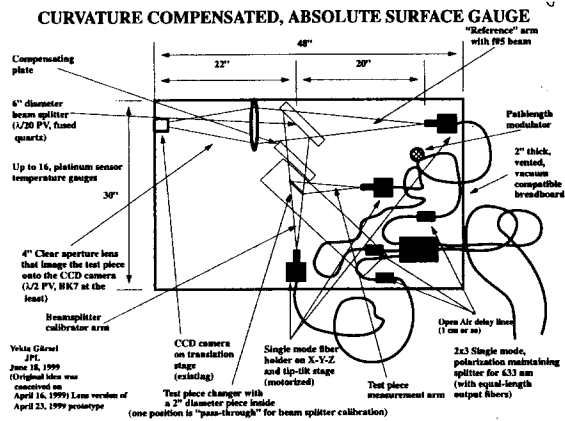


Figure 8. Left: Optical diagram of the 3-fiber gauge. Right: The picture of the 3-fiber gauge. The automatic piece changer has not yet been installed. A 3-ball, kinematic mount is used to change pieces manually.

measure flatness of reference non-curved optical pieces at that are used in the next step to measure the siderostat reflective surface to the optical-corner of the embedded retro-reflector distance to at least a nanometer.

3.1. The gauge construction

The idea² behind the 3-fiber gauge is that the wavefront emitted by a highly polished, single mode, polarization preserving optical fiber is very nearly perfectly spherical. When two such perfectly matching fibers are interferometrically combined by a beam splitter at exactly equal distances from the tips of the fibers, the resulting fringe pattern can be used to deduce the flatness of the beam splitter absolutely.

The problem of course is that the fibers do not have exactly matching wavefronts even if the distances to the beam splitter are exactly equal. However, they are likely to be much better polished than the beam splitter as the fiber tip is only a 5 microns in diameter and the beam splitter is 30,000 times larger. So, what one gets from the measurement above is a calibration of the beam splitter with respect to the very small errors (much less than 1 part in 1000) caused the fiber tips.

Non-curved optical piece flatness measurement using the system above requires two measurements to be made. First the beam splitter with fibers are calibrated. Then, one of the fiber beams are made to reflect from the new piece and the measurement is repeated. The two results are subtracted to obtain the absolute figure for the new optical piece.

To achieve what was described above without losing the alignment of the interferometer requires a more complicated set-up. Fig. 8 shows a diagram and a picture of the 3-fiber gauge.

A stabilized, Spectra-Physics Model 117A He-Ne laser is coupled into a single-mode, polarization preserving fiber for 0.6328 μm . The fiber enters a large, plexiglass enclosure that covers the gauge assembly. Three, 1x2 polarization preserving fiber splitter-combiners are attached to the incoming fiber to supply four outputs with equal power. Three of these outputs are attached to 1" travel open-air delay lines. The remaining output serves as a power monitor. The output of the delay lines are the three-fibers that drive the 3-fiber gauge. Two of the delay lines are powered by Newport AD-100 electrostrictive, manually adjustable actuators with at least 30 μm of electrical travel range. The remaining delay line is adjustable by a manual micrometer.

The fiber outputs are combined by a 150 mm clear aperture beam splitter and a 150 mm clear aperture compensating plate that supply 100 mm of clear aperture at 45 degrees. The unused faces of the beam splitter are coated with V-anti-reflection coatings at 0.6328 μm at 45 degrees of angle of incidence.

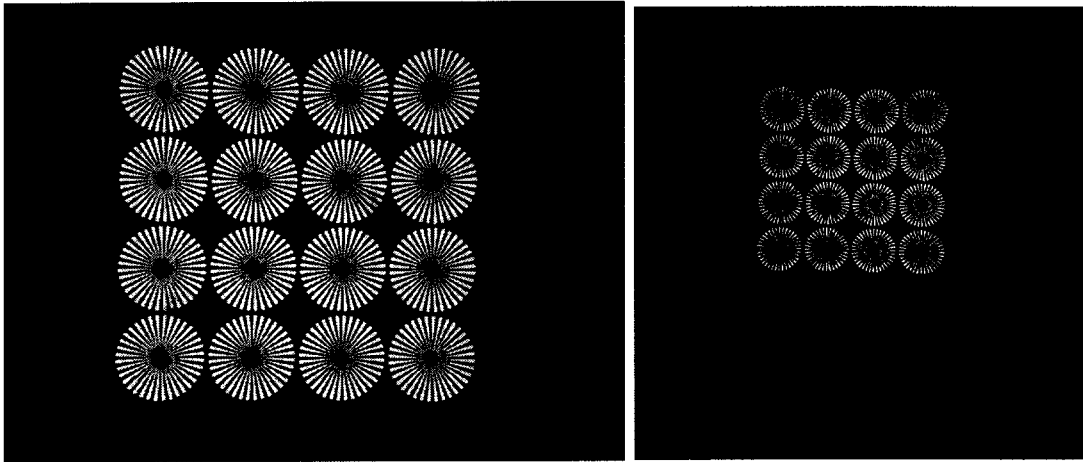


Figure 9. Left: The imaging quality of the 3-fiber gauge lens system at reduced field of view. Right: The imaging quality of the 3-fiber gauge at full field of view. The real object size in the image is 1" x 1".

The output of the beam splitter goes into an imaging system designed by the author to accommodate the f#5 diverging beam. The imaging system which is made out of two very thick, standard, off-the-shelf, double-convex lenses performs very well, supplying an 8:1 optical image size compression, and imaging the test piece on to a 1" CCD camera. The field of view of the instrument is 2" x 2" at the test piece plane with a 1000 x 1000 Kodak 10-bit, digital video camera. During the initial tests, a 640 x 480 camera at 8 bits is used at a proportionally reduced field of view. Fig. 9 shows the imaging quality with a test pattern at the test piece plane through the 3-fiber gauge imaging system. The 10-bit digital camera connects to 1 GHz Intel Pentium-IV PC or a VME crate for frame grabbing and processing. The 8-bit camera is again connected to a old 500 MHz, Intel Pentium PC III with a PCI bus compatible, Conexant Bt-848 chip based, 8-bit frame grabber. LINUX operating system with the readily available device drivers (bttv) complete the data system. The data is collected at the size of 640 x 480 by 8 bits, at the rate of 16-to 24 frames per second. All frames are saved directly to disk without compression. A typical run of 1 hour is about 25 GB. The data is analyzed on the same PCs by algorithms developed solely by the author.

3.2. The interferometer alignment and phase-shifting

There are two separate alignments to be performed. First, the two fibers that calibrate the beam splitter and the compensating plate system are aligned to each other. This involves first aligning the beam splitter and compensating plate parallel to each other. Then, the fibers are aligned to get completely circular fringes using the stabilized laser light. Next, a laser-diode is connected at the input and its frequency is swept while adjusting the separation between one of the fiber tips and the beam splitter until the fringes flatten out. This is a very delicate part of the alignment as non-parallelism between the beam splitter and the compensating plate manifests itself as astigmatism error on the phase maps and all adjustments are tiny compared to the full adjustment range.

Next, the fiber that illuminates the test piece is aligned to the reference fiber. For this alignment, the test piece is inserted in the beam path and the corresponding fiber is aligned to the reference fiber using only the new fiber degrees of freedom and the degrees of freedom of the test piece holder. The procedure for equalizing the path-lengths is the same as above. Fig. 10 shows the fringes from the test piece arm of the interferometer with circular fringes with some unequal path-length error and nearly equal path-length case with a small amount of astigmatism.

The phase-shifting is accomplished by actuating the electrostrictive element on the reference fiber delay line. A 16 bit, digital to analog converter is used through a VME crate to supply a linear ramp. The ramp is

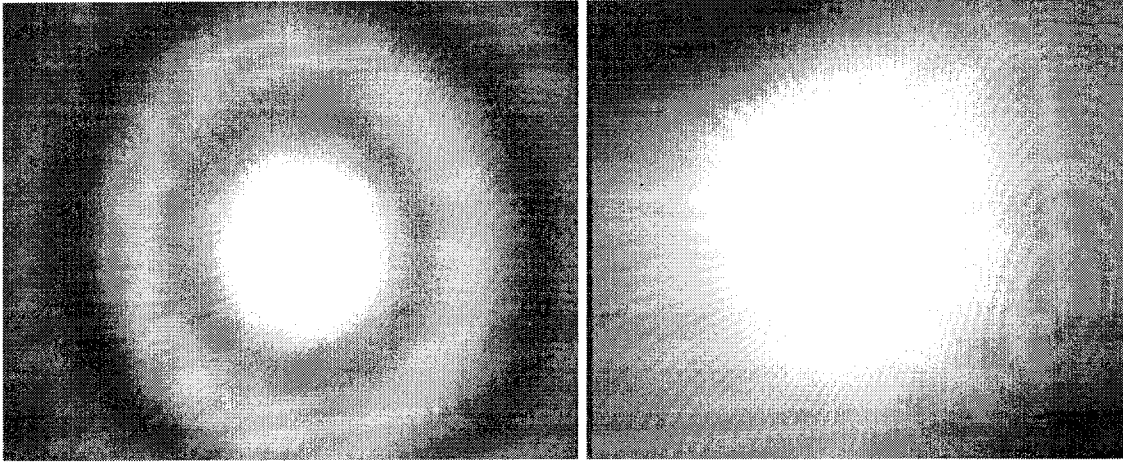


Figure 10. Left: The circular fringes near optimum alignment. This is the test piece arm of the interferometer. Right: The near-flat fringes near optimum alignment. This again is the test piece arm of the interferometer.

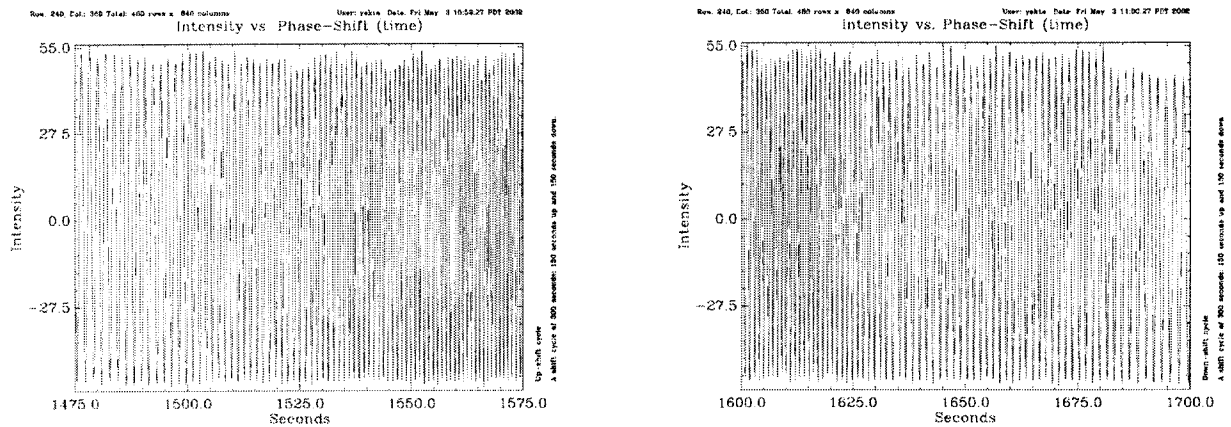


Figure 11. Left: An up-shift region for the central pixel. Right: A down-shift region for the central pixel.

amplified by a linear high voltage amplifier before it is applied the actuator. The actuator moves the delay line back and forth with an amplitude of about 36 microns, taking about 336 seconds to go through a cycle.

3.3. Data analysis

The data come out of the frame grabber as time-tagged sequential frames. The data rate may vary depending response time of the digitizing computer, hence the data is not equally spaced, but it is correctly time tagged. After the data is collected, the analyzing computer sorts the time tags and makes a time-line. The data is then converted from a video-frame-first format to a depth-first format in which a pixel is traced through the entire time line. The operation is repeated for every pixel.

This particular format prevents the computer from scanning over the entire data set every time a pixel is analyzed for phase. The scanning over the frames is decoupled from the analysis and it is performed fewer times depending on the memory size of the analyzing computer.

For each of the alignments shown in Fig. 10, the 3-fiber gauge has been run for about 1 hour and a half that resulted in 27 phase maps. These phase maps are subtracted from each other to determine the gauge repeatability and its time dependence. Fig. 15 shows a difference map in 3-dimensions and its contour representation.

3.4. Gauge repeatability

The entire depth-first data is analyzed using the algorithm described above. The output is a wrapped phase map that is calibrated in surface height. This map is then un-wrapped using a complicated noise-tolerant unwrapping-algorithm that keeps track of the quality of the fit and other physical parameters. Fig. 14 shows the wrapped and then subsequently un-wrapped phase map in the case of circular fringes shown in Fig. 10.

Figure 15. Left: The difference map between Map 1 and Map 3. Run value is 0.0015 λ . Right: The contour representation of the map on the left.

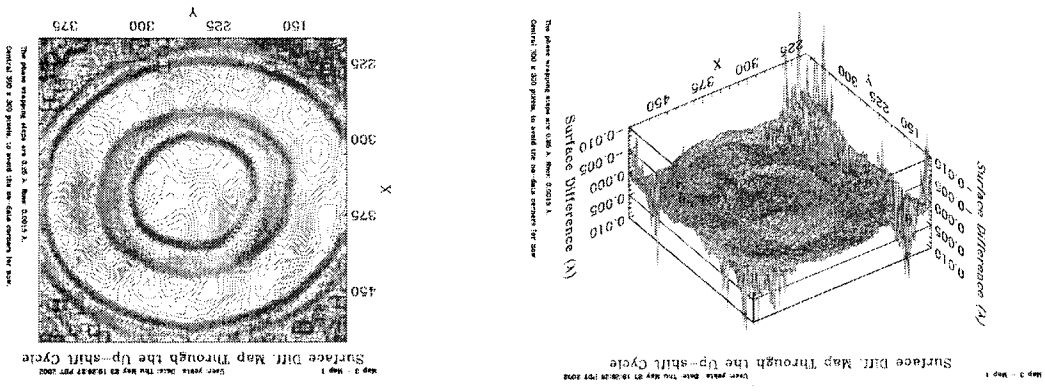
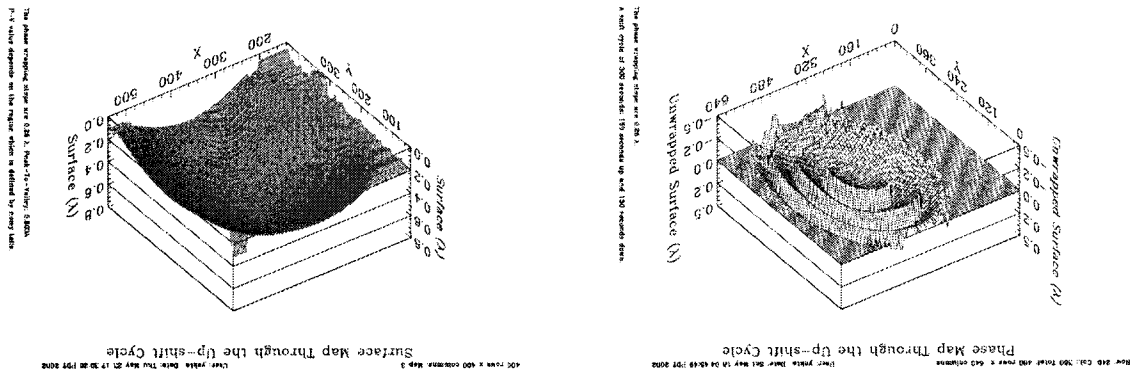


Figure 14. Left: The wrapped phase map corresponding to the circular fringes shown in Fig. 10. Right: The un-wrapped phase map corresponding to the circular fringes shown in Fig. 10.



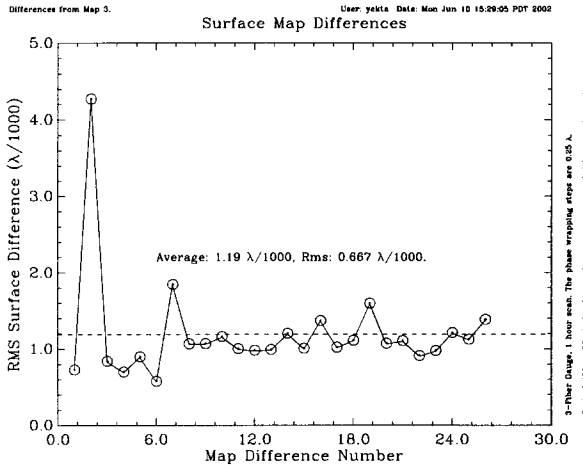
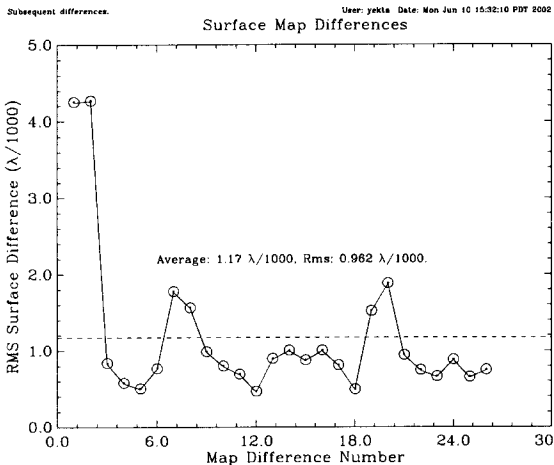


Figure 16. Left: The rms value of the difference map between two subsequent maps as a function of the map number (time). Right: The rms value of the difference map from the map number 3 as a function of the map number (time).

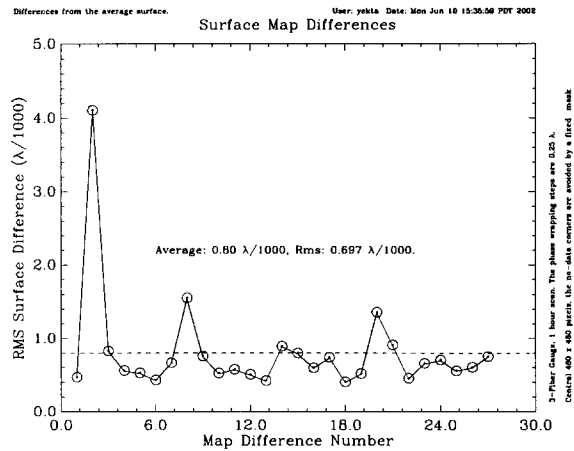
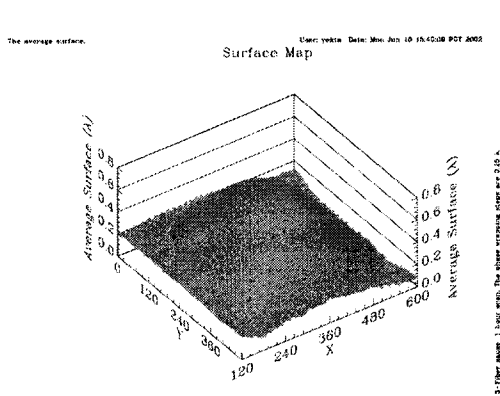


Figure 17. Left: The average surface map derived from all 27 maps for the alignment shown in Fig. 10. Right: The rms value of the difference map from the average map (left) as a function of the map number (time).

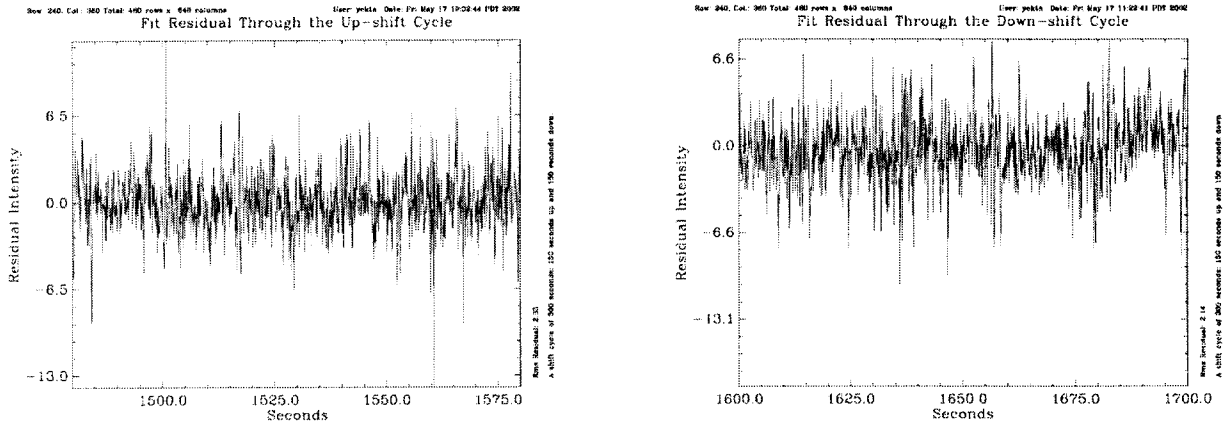


Figure 12. Left: The residual of the variable parameter sinusoidal fit for the central pixel in the up-shift region. Right: The residual of the variable parameter sinusoidal fit for the central pixel in the down-shift region.

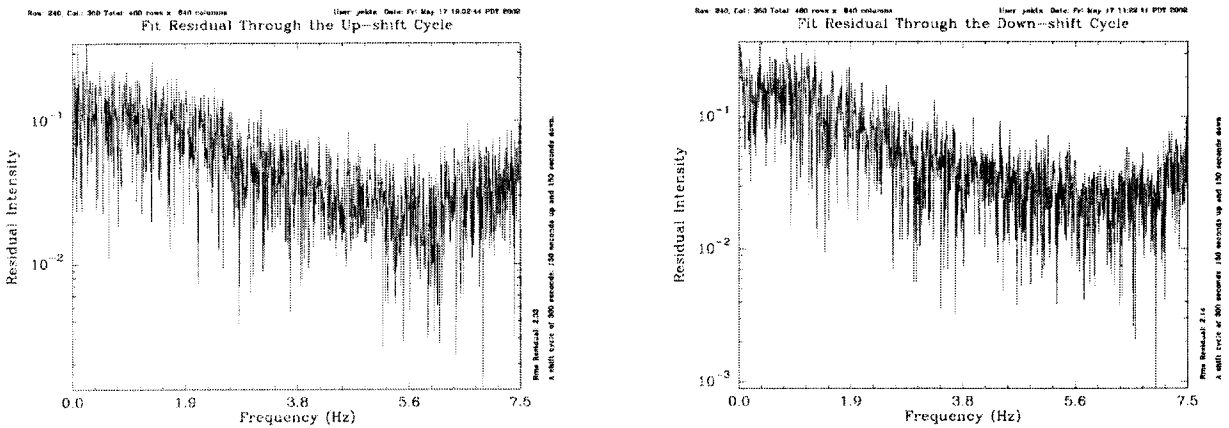


Figure 13. Left: The spectrum of the residual of the variable parameter sinusoidal fit for the central pixel in the up-shift region. Right: The spectrum of the residual of the variable parameter sinusoidal fit for the central pixel in the down-shift region.

The computer then locates the clean shift regions in the sorted data by looking at the central pixel data. These are the “sides” of the triangular-wave ramp away from the corners where the actuation actually stops for a while by design. This algorithm is like the automatic-music-search algorithms most tape recorders employ by looking at the gaps between the songs. Fig. 11 shows two subsequent shift regions (up-shift and down-shift) in which the velocity of the actuation increases and then decreases respectively. This is due to the non-linearity of the Newport actuator. The amplitude of the nearly sinusoidal fringe goes up and down due to polarization rotation. Fibers expand and shrink causing unpredictable changes in the fringe temporal frequency and shape.

The author has developed an algorithm that can fit through all of this and track the surface phase with ease. The algorithm is based on a zero-crossing initialized variable frequency and amplitude sinusoidal function fit which completely avoids over-fitting. The residuals of the fit are shown in Fig. 12. All relevant information is extracted leaving only the noise that can not be avoided. Fig. 13 shows the residual in the frequency domain.

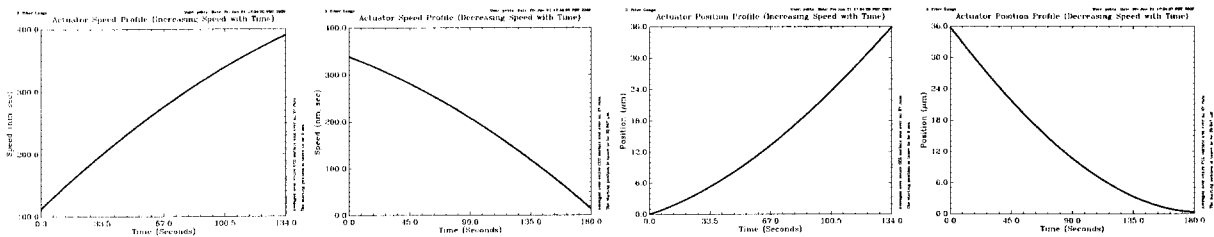


Figure 18. The actuator-velocity and actuator-position curves for up-shift and down-shift regions respectively.

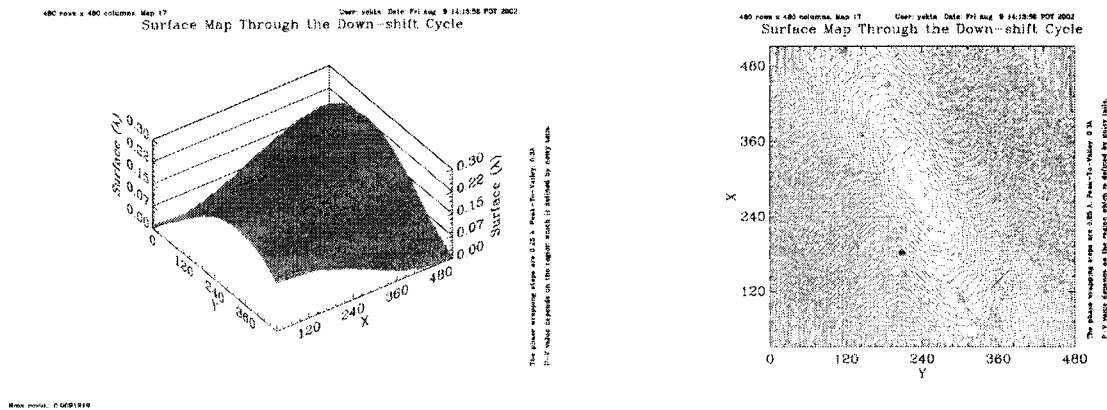


Figure 19. Background curvature with better alignment. The peak-to-valley value is now only 0.3λ .

There are several measures of repeatability. One is to compute all subsequent differences between the maps and plot them out as a function of time (map number), showing what is changing from one moment to the next. Another is to compute differences from one fixed map showing what drifts as time goes on. Finally, one can define an average map which is the best estimate of what the real map is like, and the compute differences from that one, showing mostly the random fluctuations in the system. Fig. 16 and Fig. 17 illustrate these measures of repeatability. The very large deviation near the beginning in the rms value charts is caused by map 2 which is exceptionally noisy due to the environmental vibrations near the beginning of the run. The rms deviation from the average surface is about $\lambda/1500$ at the wavelength of $0.6328 \mu\text{m}$. The peak-to-valley background curvature is slightly under 0.8λ .

3.5. The actuator non-linearity

The delay-line phase-shift actuator velocity and position curves also come out as a by-product of the first run. These data are programmed into the actuator driver computer to make the next run more linear. Fig. 18 shows the actuator velocity and actuator position curves for up-shift and down-shift regions respectively.

3.6. Background curvature reduction

The only remaining problem is the reduction of the background curvature which is about 0.8λ as shown in the first part of Fig. 10. A short optimization resulted in the fringe pattern that is shown in the latter part of the same figure. A new run is performed with the now-linearized actuator drive. The resulting background curvature is shown in Fig. 19. The peak-to-valley value is now 0.3λ .

The repeatability has also improved to $\lambda/1800$ with much less systematic errors. Fig. 20 illustrates this. The sole limitation to the alignment problem is the actuator resolution in the mounts and the researchers patience.

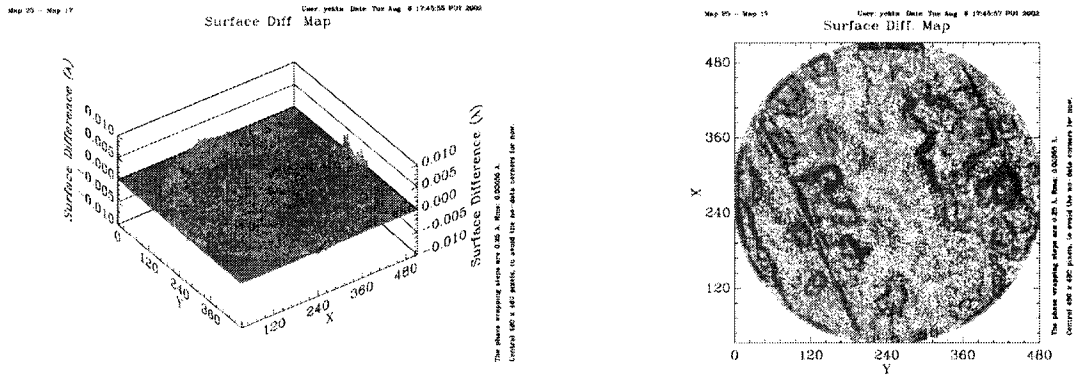


Figure 20. The difference between two subsequent maps in the newest run. Its rms value is smaller and it has much less systematic noise.

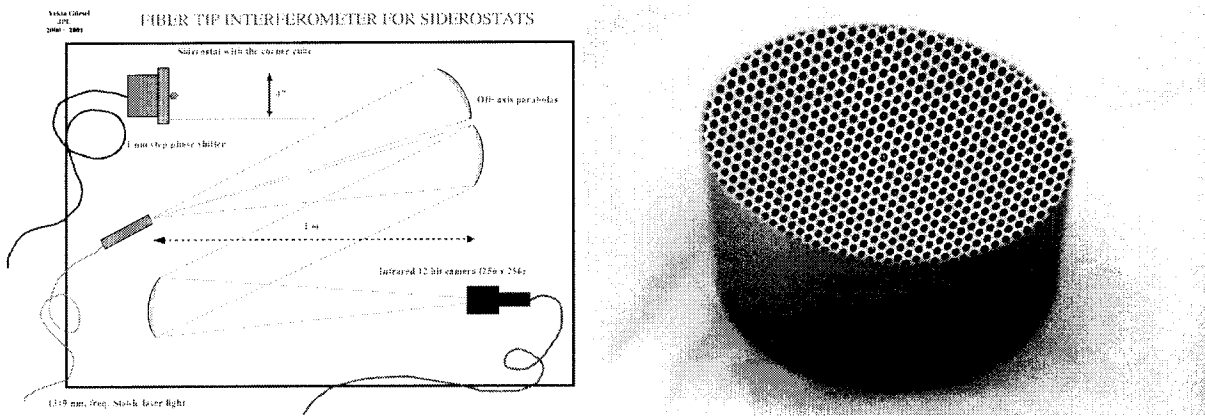


Figure 21. Left: The diagram of the split fiber gauge. Right: One of the zerodur off-axis parabolas. The regular pattern reflecting off it clearly shows the off-axis curvature.

The gauge stays aligned for weeks on end if it is left alone. There was one instance when someone had misaligned it, just before this conference. The author restored it to its original alignment.

The results of absolute measurements of a flat piece using the 3-fiber gauge will be reported in a subsequent paper.

4. THE SPLIT FIBER-BEAM GAUGE

The split fiber-beam gauge uses the calibrated flat in the 3-fiber gauge to measure the separation of siderostat reflective-surface and the optical corner of the retro-reflector in a siderostat-retro-reflector assembly. Fig. 21 shows a diagram of the split fiber-beam gauge. The $f\#5$ beam from a single mode, 1319 nm fiber is split in half by a pair off-axis parabolas. One half of the beam is collimated and falls on the siderostat-retro-reflector assembly. The returned beam is focused by the same parabola and it is sent back toward the fiber. It reflects off the core surface of the fiber and interferes with the other half of the beam coming out of the fiber. The interfering divergent beams are caught by the other parabola and send to an infrared, 12 bit, 256 x 256 camera

for fringe analysis. The phase shifting is performed by 10 nm stepping accuracy and 1 nm resolution, closed loop, three-axis piezoelectric transducer.

Since open of the parabolas are in the interferometer path, the system needs to be calibrated. This is accomplished by replacing the siderostat-retro-reflector assembly by the flat calibrated in the 3-fiber gauge.

All parts for this system are procured. Fig. 21 also shows one of the zerodur, off-axis parabolas. The regular hole pattern reflecting off the surface clearly shows the off-axis curvature. The interferometer is in the assembly phase.

5. CONCLUSION

The Stellar Interferometry Mission (SIM), and particularly one of its testbeds [the Micro-Arc-Second Metrology Testbed (MAMTB)] require compound optical pieces the construction and qualification of which, in turn, require very high-precision absolute surface metrology gauges.

We have built a white-light assembly interferometer and assembled two siderostat-retro-reflector combinations with less than 50 nm separation between the siderostat reflective-surface and the optical corner of the retro-reflector. Previous attempt by others had yielded 100 times larger separations.

We have also built a 3-fiber gauge which will be used to measure an optical flat absolutely. The gauge has attained a repeatability of $\lambda/1,800$ in air. The calibrated flat will then be used in the split fiber-beam gauge to measure the separation between the siderostat reflective-surface and the optical corner of the retro-reflector to fractions of a nanometer in vacuum. The split fiber-beam gauge is under construction.

ACKNOWLEDGMENTS

I would like to thank M. Shao for many fruitful discussions. B.C. Holmes designed the siderostat holding flexures, retro-reflector flexure push-rod, and the siderostat to mirror mount adapter in the white-light assembly interferometer. He personally applied the glue to the aligned siderostat-retro-reflector assemblies while the author compensated for any changes in the alignments.

The research described was performed at the Jet Propulsion Laboratory, California Institute of Technology, under a contract with the National Aeronautics and Space Administration.

REFERENCES

1. E. Schmidtlin and S. Shaklan, JPL mam-lib docushare internal library, *mam-lib.jpl.nasa.gov/Engineering Documents/MAM1/Alignment/CC-Sid alignment images*, November 11, 2000.
2. F. Snell, D. Phillion, G. Sommargren, and E. Campbell, New Interferometer Measures to Atomic Dimensions, in *Science and Technology Review, Lawrence Livermore Laboratory, University of California*, p. 6-7, October 1997.
3. B.C. Holmes, Private communication, December-April 2002.
4. B.E. Hines, C.E. Bell, R. Goullioud, R. Spero, G.W. Neat, T.J. Shen, Micro-arcsecond metrology (MAM) testbed overview, in *Proceedings of SPIE Conference on Interferometry in Space*, Vol. 4852, 2002.